Journal of Flow Chemistry (2022) 12:247–254
https://doi.org/10.1007/s41981-022-00224-2

COMMUNICATIONS

Continuous diameter increase reactor – a reactor concept for maximizing productivity by a controlled diameter extension

Marcus Hafner[1] · Fabian Wolff[1] · Thorsten Roeder[1]

Received: 15 December 2021 / Accepted: 9 April 2022 / Published online: 2 May 2022

Abstract

This paper presents a novel theoretical approach for maximizing productivity in microreactors by a controlled extension of the tube diameter. A one-dimensional numeric model was developed where the tube diameter increases based on the reaction heat to achieve a constant temperature throughout the reactor length. Through this approach, a basic plug flow reactor model for mass and heat transfer was used with an integrated algorithm for a controlled diameter extension. A parametric study was performed to ensure safe operating conditions concerning thermal runaway. The results show an increase in productivity of approximately 42% for the fictional second-order test reaction.

Keywords Microstructured reactors · Tubular reactor · Process intensification · Process control · Model-based scale-up · Numerical evaluation

Introduction

Flow chemistry in microreactors offers many benefits over conventional batch chemistry. The high surface-to-volume ratio provides high heat transfer coefficients, which are the key to temperature control [1–3]. Improved temperature control also translates into higher productivity, as an overall higher process temperature can be achieved safely. In some instances, increased selectivity can be achieved [4]. Furthermore, this approach also allows process intensifications and still guarantees a safe and controlled operation due to minor hold-ups [1, 2, 5]. The small dimensions allow for short diffusion paths and thus result in fast mixing [1, 3, 6].

Traditionally, microreactors were constructed either as a coiled tube or were milled from a plate of metal or glass. As shown by several authors in [6, 7], several different microstructures can be milled from a metal plate. For example, these microstructures include temporary diameter constrictions or baffles to improve mixing. To complete the construction of a microreactor, a second top plate is then pressed and screwed tightly on the bottom plate to seal the microreactor channels [7]. The coiled tube, on the other hand, can be wound in different configurations to increase the effect of Dean flow. A common approach is to change the direction of the winding every couple of turns, as shown by the examples in [6].

The continuous improvement of additive manufacturing (3D printing) of metals, especially the reduced surface roughness, has allowed the printing of microstructured reactors with shapes and sizes previously unimaginable. Internal diameters of 0.6 mm are achievable using selective laser melting (SLM) [8, 9]. As a result of this study, a reactor shape is proposed that could be easily achieved using modern additive manufacturing techniques.

Inherently, tubular microreactors are not well suited for very long reaction times. While the reaction rate is very high in the beginning due to the high concentration of the reactants, it slows down rapidly toward the end as the concentration of the reactants decreases. This results in a rapid increase in conversion, high heat production for exothermic reactions and a temperature rise at the beginning and a slow increase in conversion, decreasing heat production and a temperature decrease toward the end. Additionally, the high surface-to-volume ratio of microstructures further benefits heat removal. The Arrhenius law predicts slower reaction rates at lower temperatures, which inevitably results in changing process conditions along the reactor. In addition to the tendency of clogging, the most significant limiting factor of microstructured

✉ Thorsten Roeder
t.roeder@hs-mannheim.de

[1] Institute of Chemical Process Engineering, Mannheim University of Applied Sciences, Paul-Wittsack-Straße 10, 68163 Mannheim, Germany

reactors is the high pressure drop accompanying high volumetric flow rates [2, 6].

There are several approaches to choose from to overcome this weakness and provide more constant process conditions. These approaches can either influence the concentration of the reactants or influence the temperature at which the reaction is taking place. A widespread way to manipulate the concentration is by using a multi-injection solution, where the concentration of the reactant is increased successively at specific lengths of the reactor by injecting fresh reactants, thus increasing the reaction rate. To influence the temperature at which the reaction takes place, the reactor can be separated into different zones, each in a different temperature zone than the previous zone. For example, a coiled tube is immersed in different cooling baths, each with a higher temperature than the previous bath.

The second option for optimizing the temperature profile in the case of highly exothermic reactions is a stepwise increase in the tube diameter at specific reactor lengths. As shown in Fig. 1, this results in an abrupt decrease in heat removal capacity, thus allowing the temperature to rise and the reaction rate to accelerate. This approach also reduces the equipment needed to set up different temperature zones. With the goal of maintaining the process conditions, i.e., a constant temperature, the stepwise diameter increase could be applied in small steps throughout the reactor length. A visual representation of the approach can be seen in Fig. 1. In theory, this approach should increase productivity while providing a constant temperature throughout the reactor. This temperature control is especially beneficial for producing temperature-sensitive products such as nitroaromatic compounds, which are temperature-sensitive and degrade exothermically. An increased diameter also positively affects the pressure drop and reduces the tendency of clogging. The presented approach is not restricted to just one constant temperature profile. Additionally, any conceivable temperature profile can be employed to perform further optimizations, such as selectivity.

As presented in this paper, a numeric model was built for obtaining a tubular wall profile of the proposed continuous diameter increase reactor (CoDIR) introduced in Fig. 1. This reactor shape was optimized for a specific exothermic reaction based on specific system conditions with the goal of keeping the temperature constant throughout the reactor. Afterward, we investigated this system for parametric sensitivity by systematically sweeping sensitive parameters.

Methods

To model the plug flow reactor (PFR), a fictional exothermic organic liquid phase irreversible second-order reaction is chosen.

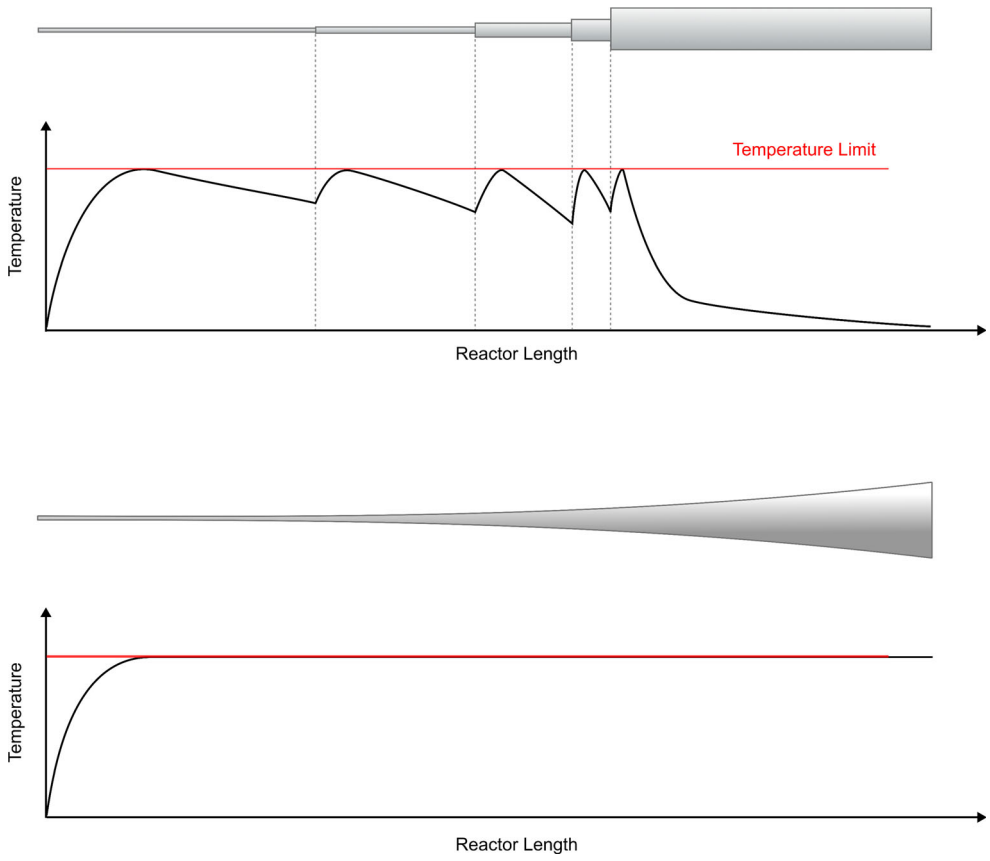

Fig. 1 Comparison between the stepwise tube diameter extension (top) and the continuous diameter increase reactor (CoDIR) (bottom)

$$A + B- > C.$$

Furthermore, an ideal plug flow is assumed. This assumption is further discussed in the Results section.

The mass balance is calculated as a change in concentration over a length. This formula is derived from the basic mass balance formula found in [10].

$$\frac{dc}{dz} = \frac{r}{u} \tag{1}$$

The reaction rate for all components in this system is the same; it has a negative prefix for the starting materials as they are used up and a positive prefix for the product as it is generated.

The reaction rate r is calculated with the following equations [10]:

$$r = k\, c_A\, c_B \tag{2}$$

$$k = k_{ref}\, e^{-\frac{E_A}{R}\left(\frac{1}{T_i}-\frac{1}{T_{ref}}\right)} \tag{3}$$

The temperature-dependent reaction rate is calculated by applying the Arrhenius law to the fictional reaction rate constant k_{ref} at a temperature of 293.15 K.

The equation for the energy balance used here is modified to use the density and mean flow velocity instead of the area in the source part. The basic equation can be found in [10].

$$\frac{dT}{dz} = \frac{r(-\Delta H_R)}{\rho\, u_i\, c_p} + \frac{k_W\, \pi\, d\, (T_W - T_i)}{\dot{m}\, c_p} \tag{4}$$

The flow inside the reactor is laminar with a very low Reynolds number; thus, a Nusselt number of 3.656, which represents the edge case of laminar flow, is applied here. This means that the heat transmittance k_W will be limited by the heat transfer on the process side α_i, so the heat conduction through the tube wall and the heat transfer to the cooling liquid can be neglected.

As shown in [11], the hydrodynamic and thermal entry length can be estimated by the following Eqs. (5) and (6):

$$L_{hyd.} \approx 0.05 \cdot Re \cdot d \tag{5}$$

$$L_{th.} \approx 0.05 \cdot Re \cdot d \cdot Pr \tag{6}$$

In the following table, the constants used for the second-order kinetics and the material properties for the product side are shown (Table 1):

Solving the differential equations for a finite length dz. is beneficial for our model because the reactor is discretized into thin slices of a given thickness dz. The mass and heat balances are then solved numerically inside the slice over its thickness.

The differential equations are solved for a slice n based on the initial conditions in the model. The results of slice n are the initial conditions for slice n + 1. The very first slice is calculated with the chosen starting conditions. The solution continues until all slices are calculated. After that, the data are evaluated, and the reactor is cut after the slice where a 90% conversion rate is reached.

Table 1 Material Properties

Parameter	Value	Unit
R	8.314	$J/(mol \cdot K)$
E_a	50.00	kJ/mol
k_{ref} (293.15 K)	2.00E-05	$m^3/(mol \cdot s)$
$\Delta_r H$	−150.0	kJ/mol
ρ	786.4	kg/m^3
η	0.0023	$Pa \cdot s$
c_p	153.6	$J/(kg \cdot K)$
λ	0.1365	$W/(m \cdot K)$

Algorithm for the diameter extension calculation

In the first step, the reaction system is solved for a regular PFR model with a constant diameter. The resulting maximum temperature is the benchmark temperature we aim to hold constant throughout the CoDIR. Therefore, we aim to achieve an isothermal mode of operation for the model by increasing the diameter and thus decreasing the heat transfer coefficient due to their reciprocal relationship. The temperature difference between the reference and the slice temperature is fed into a PID controller, which subsequently calculates a new reactor shape for each slice. If the temperature of the slice is lower than the benchmark, then the output increases the diameter, which leads to a temperature increase in the next slice. Alternatively, the slice diameter is calculated by solving Eq. (4) with $dT_i/dz = 0$, as seen in the supporting material. In this publication, the PID approach is chosen because it opens the opportunity to create even more complex temperature profiles, such as several temperature zones along the reactor length. Furthermore, to avoid oscillations of the diameter, the diameter is changed only when the temperature decreases from slice n to slice n + 1 or does not change. Therefore, the diameter can only remain constant or increase.

Figure 2 shows a flow chart of the CoDIR algorithm steps.

Results and discussion

An implementation of the algorithm previously described in the Methods section was developed (MATLAB). The process conditions used as base parameters for the simulation are listed in Table 2. The reactor wall is assumed to be at a

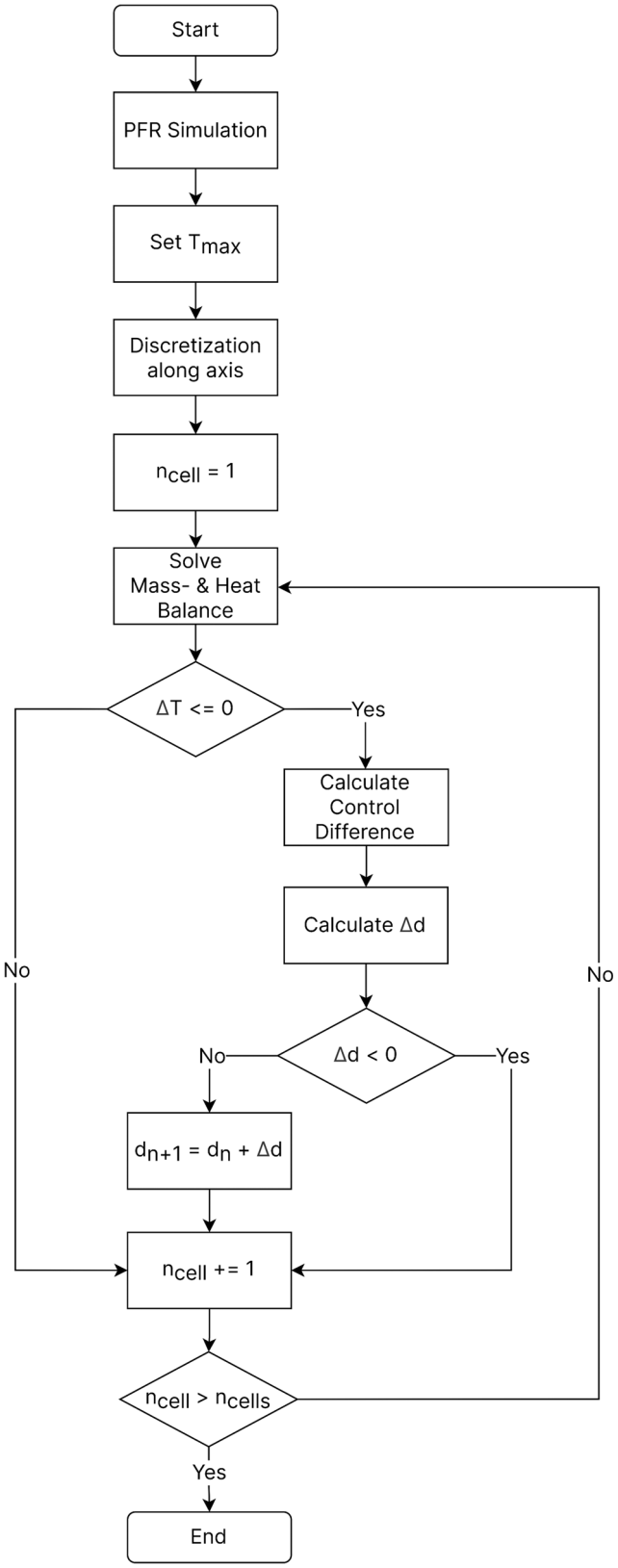

Fig. 2 Algorithm flow chart

constant temperature of $T_W = 20\ ^\circ C$. Together with the material properties in Table 1, the parameters were selected to resemble a typical setup for fast, highly exothermic aromatic nitration, according to Westermann et al. [12]. Highly exothermic aromatic nitration reactions are one example of reactions that can be performed very efficiently in microreactors [13].

Table 2 Reference process conditions

Parameter	Value	Unit
T_0	20	$°C$
T_W	20	$°C$
C_{A0}	3500	mol/m^3
C_{B0}	3500	mol/m^3
C_{C0}	0	mol/m^3
$\dot{V}$	0.1	ml/min
d_i	0.5	mm

The data presented in Fig. 3 through Fig. 7 show the reactor behavior up to a 90% conversion. Additionally, a comparison between the results of the regular PFR and CoDIR is carried out. Figures 3 and 4 show the resulting temperature and conversion profiles for both scenarios. The resulting PFR has a volume of $V_{PFR} = 0.207\ ml$, while the CoDIR has a volume of $V_{CoDIR} = 0.146\ ml$. Since for both cases, a constant flow rate of $\dot{V} = 0.1\,\frac{ml}{min}$ is assumed, the reaction inside the CoDIR results in an overall shorter residence time of $\tau_{CoDIR} = 87.6\ s$ compared to the residence time $\tau_{PFR} = 124.1\ s$ of the PFR.

As expected, the PFR shows a sharp temperature peak at the start, followed by a decrease in the reactor temperature due to the slowing down of the reaction while maintaining a very high heat removal. On the other hand, the CoDIR holds the temperature peak throughout the whole reactor at approximately $\vartheta_{max} = 25.6\ ^\circ C$, resulting in a much shorter residence time due to increased productivity according to the Arrhenius

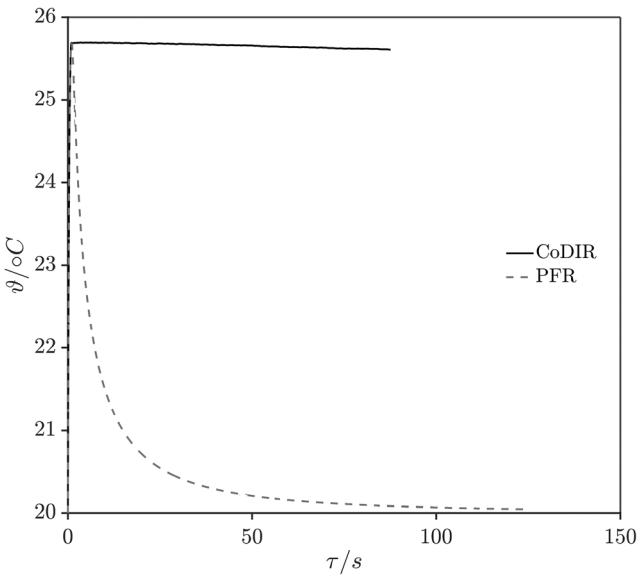

Fig. 3 Temperature vs. residence time for the CoDIR and PFR

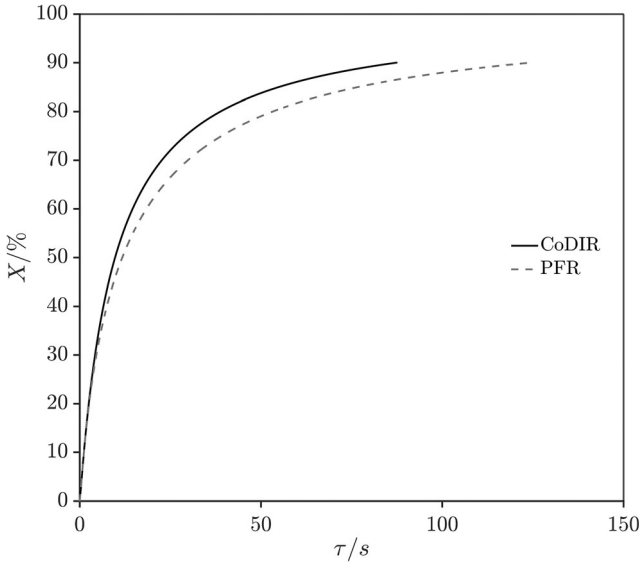

Fig. 4 Conversion vs. residence time for the CoDIR and PFR

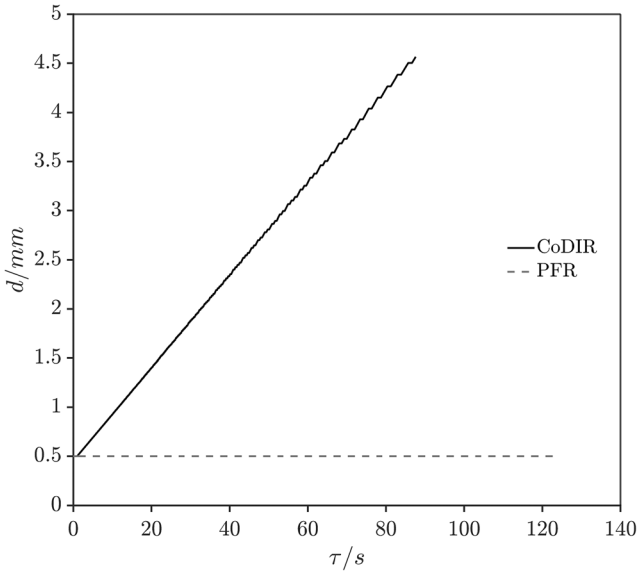

Fig. 6 Tube diameter vs. residence time for the CoDIR and PFR

law. The CoDIR provides a much higher mean temperature $\overline{\vartheta}_{CoDIR} = 25.6°C$ compared to $\overline{\vartheta}_{PFR} = 20.5°C$ while reducing the overall temperature fluctuation represented by the standard deviation $\sigma_{CoDIR} = 0.66\ K$ and $\sigma_{PFR} = 0.88\ K$. This benefits the productivity and prevents the buildup of side products due to more uniform reaction conditions. Additionally, the conversion profile also shows increased productivity along the reactor with an increased slope compared to the PFR after hitting the peak temperature.

Figure 5 shows the change in the reactor diameter along the reactor length, while Fig. 6 also shows the reactor diameter plotted against the residence time. The much shorter reactor length and higher slope result from the volume of each new volume element drastically increasing due to the increased diameter. Over the length of the CoDIR, a ninefold increase in the diameter occurs, which successively balances the decrease in generated heat from the reaction with a decrease in heat removal through the reactor wall. The heat removal and generation for both reactors can be found in the supporting material.

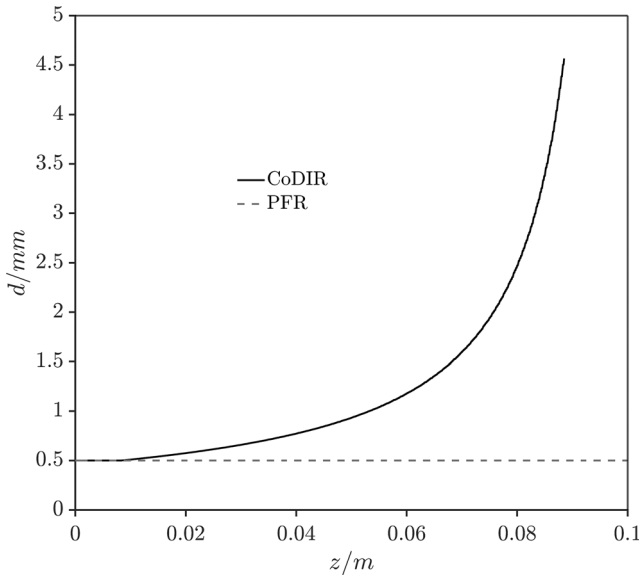

Fig. 5 Tube diameter vs. reactor length for the CoDIR and PFR

An overall comparison of the test scenarios described in the Methods section is shown in Table 3. The calculated space-time yield for the CoDIR increases by approximately 42% for the fictitious test reaction compared to the PFR, while the residence time decreases by approximately 30%. This shows the overall effectiveness of the proposed approach.

Reactor stability analysis

As described in the introduction, there exists a risk, especially for highly exothermic, fast reactions with high activation energy, that during the startup of the reaction, an uncontrolled generation of heat occurs (thermal runaway). In this case, the generated heat exceeds the removed heat, which leads to an uncontrolled acceleration of the reaction and starts a feedback loop. The effect of thermal runaway can hold inherent safety risks due to pressure buildup leading to violent explosions. Especially in the case of flammable and highly toxic components, this scenario must be avoided [14, 15]. Since the concept of the CoDIR decreases heat removal with progressing

Table 3 Comparison of the CoDIR and PFR simulation results

	L m	V_R ml	τ s	STY kg/(m³·h)
PFR	1.05	0.207	124.1	10960
CoDIR	0.0885	0.146	87.6	15540

reactor length to reach higher productivity, the risk of thermal runaway could be amplified, creating unstable reaction conditions. This scenario is of particular concern, and insurance of safe reaction conditions during diameter extension was thoroughly tested. The simulation, as described in the Methods section, was used to cover a change in the parameters listed in Table 4. The parameters were chosen according to their critical influence on heat removal and generation. A particular focus is placed on the effect of the activation energy with its strong nonlinear dependency within the Arrhenius law. In each simulation, the extracted optimum wall profile for the base case of the reactor was used. The base case parameters were varied for a 10 and 20% increase/decrease in the given parameter. Graphs for all parameter pairs can be found in the supporting material.

None of the parameter studies presented resulted in a thermal runaway of the process. Therefore, a general stability of the process can be concluded. Figure 7 shows a change in the activation energy of the reaction. To better view the temperature peak, the y-axis was rescaled to start at 24.5 °C, although the reaction starts at 20 °C.

The base case for the given wall profile shows a nearly constant temperature after hitting the peak temperature. As expected for higher activation energies, the reaction accelerates much faster, leading to heat generation exceeding the heat removal and resulting in a higher maximum temperature. This leads to a higher conversion early on, followed by a decreased reaction rate afterward, explaining the undershooting compared to the base case. In contrast, a lower activation energy leads to a lower temperature peak and overshooting of the temperature with progressing residence time. It is also clear that for a 20% increase in the activation energy, there is no thermal runaway, and stable reaction conditions are ensured.

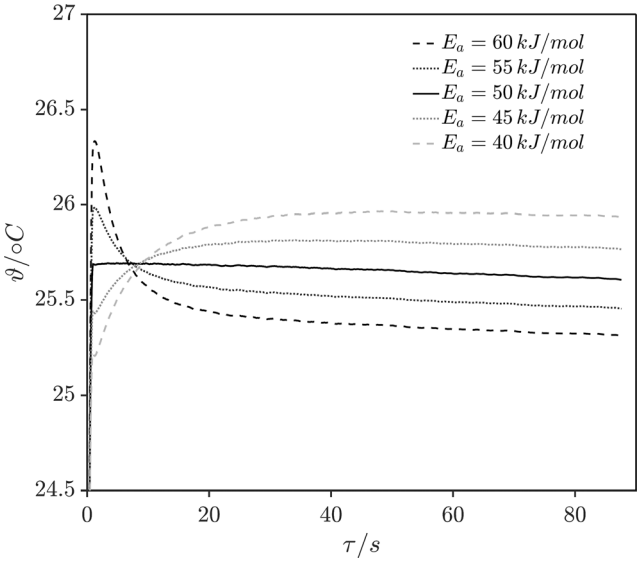

Fig. 7 Activation energy sweep, conversion vs. residence time

Discussion of assumptions and limitations

Since the diameter of the CoDIR increases by a factor of approximately 9 (from 0.5–4.6 mm) along the reactor, it should be discussed to what extent the model assumptions are appropriate and which limitations exist.

A critical parameter in our model is the Nusselt number. As the Reynolds number for the initial diameter of 0.5 mm is 1.4, the laminar flow edge case for a Nusselt number of 3.656 can be assumed. This results in a heat transmittance of 998 $W/(m^2\,K)$ for the initial diameter. In the case of heat transfer in laminar flow regions, heat transport only occurs by thermal conduction. Therefore, the Nusselt number for a laminar system is the lowest possible value. Throughout the reactor, the Reynolds number further decreases as the volumetric flow rate is held constant and the diameter increases. Thus, safe operation as a result of the ninefold diameter increase is not expected. Furthermore, for a real reactor system, the Nusselt number can be easily enhanced by inducing secondary flow with internals such as static mixers, chicanes, or zigzag channels.

Assuming fully developed hydrodynamic and thermal profiles for the entire reactor is applicable if the hydrodynamic and thermal entry lengths are significantly smaller than the total length of the reactor. Using Eq. (5), a hydrodynamic entry length of 0.035 mm is calculated, and using Eq. (6), a

Table 4 Overview of all parameters for the parametric sweeps

	E_a kJ/mol	k_{ref} $m^3/(mol \cdot s)$	$\Delta_r H$ kJ/mol	$\dot{V}$ ml/s	T_W $°C$	$C_{A,0}/\ C_{B,0}$ mol/m^3	n_α $-$
−20%	40	1.60E-05	−120	0.08	16	2800	0.8
−10%	45	1.80E-05	−135	0.09	18	3150	0.9
base	50	2.00E-05	−150	0.1	20	3500	1
+10%	55	2.20E-05	−165	0.11	22	3850	1.1
+20%	60	2.40E-05	−180	0.12	24	4200	1.2

thermal entry length of 1.6 mm is calculated. Both values are several orders of magnitude smaller than the reactor length of approximately 89 mm [11]. With regard to heat transfer, compared to the fully developed region, the thermal entrance region shows an intensified heat transfer rate.

Notably, for a reactive system, the Nusselt number would be higher than that predicted for the laminar edge case [3]. As a higher Nusselt number leads to a faster drop in temperature, the risk of thermal runaway further decreases.

Plug flow can only be assumed for tubular channels if radial compared to axial diffusion is sufficiently high [16]. In general, plug flow provides a good representation of the prevailing flow regime in microreactors due to small tube dimensions and therefore short radial diffusion paths compared to axial ones. The dispersion model describes the degree of local back mixing for laminar flow in circular microchannels [16]. Axial dispersion can be calculated according to Taylor & Aris as a function of the tube radius, the mean velocity, and the coefficient of molecular diffusion [17–19]. As a result of the ninefold diameter increase throughout the CoDIR, the radial diffusion time increases by approximately a factor of 81 toward the end of the reactor [20]. Especially in the later stages of the CoDIR, plug flow behavior can therefore probably only be achieved by enhancing radial dispersion, e.g., by installing additional mixing elements such as static mixers [21, 22], chicanes [23], coiled flow inverters [24, 25] or zigzag channels [26, 27].

Regarding mass transfer, the model assumes one ideally mixed reactant phase. Therefore, the reaction rate is not limited by mass transport and is only dependent on the intrinsic reaction kinetics. Since liquid phase nitration reactions often involve multiphase systems, mass transfer limitations affect the reaction kinetics and would have to be taken into account [13, 28].

Furthermore, a simplified fictitious second-order reaction is used without side reactions taking place. The principle of the CoDIR can thus be illustrated in a manner that is decoupled from the chemistry. However, the improvements in productivity obtained in this way do not accurately represent the results obtained experimentally. A tendency toward increased productivity, however, is also given in practice.

An independent parameter variation was performed to evaluate the degree of parametric sensitivity. The results show no thermal runaway among any of the tested variables. A sensitivity analysis, according to Semenov, Gray and Renken, is a widely accepted approach to quantify this particular problem [29, 30]. Because the traditional approach cannot represent the sensitivity of the CoDIR, an adapted approach can be found in the supporting material.

Finally, the concept of a continuous diameter expansion can be used as an additional modular element in the design of microchannels. Compared to a sudden increase in diameter, a continuous increase offers significant advantages, as the productivity increases while the occurrence of temperature peaks is reduced. Additionally, the proposed approach even offers the option to optimize the selectivity of complex reaction systems. Different temperature zones could be created to inhibit specific side reactions based on deviating activation energies.

The drawback is higher simulation efforts since the optimal reactor profile must be tailored to the dedicated reactions/process. As a result, one becomes somewhat inflexible since small changes in the process require a new optimal wall profile to be simulated. Therefore, we propose a possible application of the CoDIR in ongoing production processes to boost productivity while reducing temperature fluctuations. Therefore, with technologies such as metal 3D printing, a new flexible module can be derived.

Conclusion

A numeric one-dimensional model was developed based on the governing PFR equations, proposing an approach to increasing the productivity of microreactors by a continuous diameter increase. The increase in diameter leads to an overall higher mean reaction temperature throughout the reactor while decreasing temperature fluctuations. The simulation results of the proposed CoDIR show an increase in space-time yield for a fictitious reaction of approximately 42% compared to the reference PFR. A parametric sensitivity study could confirm safe reaction conditions without thermal runaway, considering sensitive parameters in terms of heat generation and heat removal. In conclusion, a reactor concept was proposed to realize the full potential of microstructured devices in terms of productivity. The complex shape of this microstructured device is easily achieved with today's 3D printing techniques or can be approximated with pipe segments of different diameters.

List of symbols *c,* concentration (mol/m^3).; *z,* axial reactor coordinate (m).; *r,* radius (m).; *u,* velocity (m/s).; *k,* rate constant (m^3/(s mol)).; $\mathbf{E_A}$, activation energy (J/mol).; *R,* ideal gas constant (J/(mol K)).; *T,* temperature (K).; $\boldsymbol{\rho}$, density (kg/m^3).; $\boldsymbol{\Delta_r H}$, heat of reaction (J/mol).; $\mathbf{c_p}$, heat capacity (J/(mol K)).; $\mathbf{k_w}$, total heat transfer coefficient (W/(m^2 K)).; *d,* diameter (m).; $\dot{\mathbf{m}}$, mass flow rate (kg/s).; *L,* length (m).; *Re,* Reynolds number (−).; *Pr,* Prandtl number (−).; $\boldsymbol{\lambda}$, heat conductivity (W/(m K)).; $\dot{\mathbf{V}}$, volumetric flow rate (m^3/s).; $\boldsymbol{\tau}$, residence time (s).; $\boldsymbol{\sigma}$, standard deviation (−).; *STY,* space-time yield (kg/(h m^3)).

Subscripts *A,* Substance A.; *B,* Substance B.; *ref.,* Reference.; *i,* i-th slice.; *W,* Wall.; *hyd.,* Hydrodynamic.; *th.,* Thermal.; *0,* initial value; *CoDIR,* Continuous diameter increase reactor.; *PFR,* Plug flow reactor.

Supplementary Information The online version contains supplementary material available at https://doi.org/10.1007/s41981-022-00224-2.

Funding Open Access funding enabled and organized by Projekt DEAL.

Declaration

Conflict of interest The authors declare they have no financial interests.

References

1. Plutschack MB, Pieber B, Gilmore K et al (2017) The Hitchhiker's guide to flow chemistry ‖. Chem Rev 117:11796–11893. https://doi.org/10.1021/acs.chemrev.7b00183
2. Gelhausen MG, Kurt SK, Kockmann N (2015) Parametrische Empfindlichkeit einer stark exothermen Reaktion im Kapillarwendelreaktor. Chemie Ingenieur Technik 87:781–790. https://doi.org/10.1002/cite.201400141
3. Schwolow S, Ko JY, Kockmann N et al (2016) Enhanced heat transfer by exothermic reactions in laminar flow capillary reactors. Chem Eng Sci 141:356–362. https://doi.org/10.1016/j.ces.2015.11.022
4. Kockmann N, Gottsponer M, Zimmermann B et al (2008) Enabling continuous-flow chemistry in microstructured devices for pharmaceutical and fine-chemical production. Chemistry 14:7470–7477. https://doi.org/10.1002/chem.200800707
5. Hessel V, Kralisch D, Kockmann N (2014) Novel process windows: innovative gates to intensified and sustainable chemical processes. Wiley-VCH Verlag GmbH & Co KGaA, Weinheim
6. Schwolow S, Heikenwälder B, Abahmane L et al (2014) Kinetic and scale-up investigations of a Michael addition in microreactors. Org Process Res Dev 18:1535–1544. https://doi.org/10.1021/op5002758
7. Kockmann N, Gottsponer M, Roberge DM (2011) Scale-up concept of single-channel microreactors from process development to industrial production. Chem Eng J 167:718–726. https://doi.org/10.1016/j.cej.2010.08.089
8. Gutmann B, Köckinger M, Glotz G et al (2017) Design and 3D printing of a stainless steel reactor for continuous difluoromethylations using fluoroform. React Chem Eng 2:919–927. https://doi.org/10.1039/c7re00176b
9. Maier MC, Valotta A, Hiebler K et al (2020) 3D printed reactors for synthesis of active pharmaceutical ingredients in continuous flow. Org Process Res Dev 24:2197–2207. https://doi.org/10.1021/acs.oprd.0c00228
10. Fogler HS (2016) Elements of chemical reaction engineering, Fifth edition. Prentice Hall international series in the physical and chemical engineering sciences. Prentice Hall, Boston
11. Oertel H (2017) Prandtl - Führer durch die Strömungslehre. Springer Fachmedien Wiesbaden, Wiesbaden
12. Westermann T, Mleczko L (2016) Heat Management in Microreactors for fast exothermic organic syntheses—first design principles. Org Process Res Dev 20:487–494. https://doi.org/10.1021/acs.oprd.5b00205
13. Halder R, Lawal A, Damavarapu R (2007) Nitration of toluene in a microreactor. Catal Today 125:74–80. https://doi.org/10.1016/j.cattod.2007.04.002
14. Nolan PF, Barton JA (1987) Some lessons from thermal-runaway incidents. J Hazard Mater 14:233–239. https://doi.org/10.1016/0304-3894(87)87015-2
15. Kummer A, Varga T (2021) What do we know already about reactor runaway? – a review. Process Saf Environ Prot 147:460–476. https://doi.org/10.1016/j.psep.2020.09.059
16. Levenspiel O (1999) Chemical reaction engineering, 3. ed. Wiley, Hoboken, NJ
17. Taylor G (1953) Dispersion of soluble matter in solvent flowing slowly through a tube. Proc R Soc Lond A 219:186–203. https://doi.org/10.1098/rspa.1953.0139
18. Bello MS, Rezzonico R, Righetti PG (1994) Use of Taylor-aris dispersion for measurement of a solute diffusion coefficient in thin capillaries. Science 266:773–776. https://doi.org/10.1126/science.266.5186.773
19. Aris R (1956) On the dispersion of a solute in a fluid flowing through a tube. Proc R Soc Lond A 235:67–77. https://doi.org/10.1098/rspa.1956.0065
20. Atkins PW, de Paula J, Keeler JJ (2018) Atkins' physical chemistry, Eleventh edition. Oxford University Press, Oxford, New York
21. Falk L, Commenge J-M (2010) Performance comparison of micromixers. Chem Eng Sci 65:405–411. https://doi.org/10.1016/j.ces.2009.05.045
22. Brechtelsbauer C, Ricard F (2001) Reaction engineering evaluation and utilization of static mixer Technology for the Synthesis of pharmaceuticals. Org Process Res Dev 5:646–651. https://doi.org/10.1021/op010056t
23. Rojahn P, Ruß O, Gössl L et al (2020) Mixing performance in a distributed-feed plate-type reactor with multinozzle injection for fine chemical production scale. Ind Eng Chem Res 59:3655–3668. https://doi.org/10.1021/acs.iecr.9b06407
24. Klutz S, Kurt SK, Lobedann M et al (2015) Narrow residence time distribution in tubular reactor concept for Reynolds number range of 10–100. Chem Eng Res Des 95:22–33. https://doi.org/10.1016/j.cherd.2015.01.003
25. Rojahn P, Hessel V, Nigam KD et al (2018) Applicability of the axial dispersion model to coiled flow inverters containing single liquid phase and segmented liquid-liquid flows. Chem Eng Sci 182:77–92. https://doi.org/10.1016/j.ces.2018.02.031
26. Schwolow S, Braun F, Rädle M et al (2015) Fast and efficient Acquisition of Kinetic Data in microreactors using in-line Raman analysis. Org Process Res Dev 19:1286–1292. https://doi.org/10.1021/acs.oprd.5b00184
27. Mengeaud V, Josserand J, Girault HH (2002) Mixing processes in a zigzag microchannel: finite element simulations and optical study. Anal Chem 74:4279–4286. https://doi.org/10.1021/ac025642e
28. Yang L, Nieves-Remacha MJ, Jensen KF (2017) Simulations and analysis of multiphase transport and reaction in segmented flow microreactors. Chem Eng Sci 169:106–116. https://doi.org/10.1016/j.ces.2016.12.003
29. Gray P, Lee PR (1965) Thermal explosions and the effect of reactant consumption on critical conditions. Combustion and Flame 9:201–203. https://doi.org/10.1016/0010-2180(65)90068-4
30. Baerns M, Behr A, Brehm A et al (2013) Technische Chemie, Zweite, erweiterte Auflage. Wiley-VCH; Ciando, Weinheim, München